A further explore the source features of the 2016 Mw 5.9 Menyuan earthquake by empirical Green's functions and dynamic simulations: self-arresting rupture of the 2016 Menyuan event

Duyuan Xu, Wenzheng Gong, Zhenguo Zhang, Houyun Yu, Xiaofei Chen

Department of Earth and Space Sciences, Southern University of Science and Technology, Shenzhen, China

南方科技大学 SOUTHERN UNIVERSITY OF SCIENCE AND TECHNOLOGY

ESS Department of Earth and Space Sciences

1. Introduction

Exploring the mysteries of why earthquakes stop is important to understand earthquake physics and seismic hazards. Previous studies indicate that the complex fault geometries [1]-[3] and the heterogeneous material properties of the fault zone [4] can influence rupture propagation. Moreover, some propose that earthquakes may terminate their ruptures spontaneously before reaching the barriers [5], which are found in some small earthquakes [6], [7] and low-frequency earthquakes [8]. However, according to the theoretical prediction [5], the maximum magnitude of this kind of earthquake (self-arresting rupture) may reach Mw 6.0~6.5. Therefore, exploring whether this type of earthquake exists in moderate earthquakes is meaningful for understanding earthquake physics.

No evidence shows the first-order variations in the fault geometry and material properties of the ruptured zone [9]-[11] for the 2016 Mw 5.9 Menyuan earthquake. What stopped this earthquake's rupture propagation after it began rupturing is worth investigating. In this work, we first get the apparent source time functions of this event using the empirical Green's function (EGF) method. Then, the dynamic rupture simulations are used to investigate the rupture process of this earthquake as constrained by the geodetic and seismic observations.

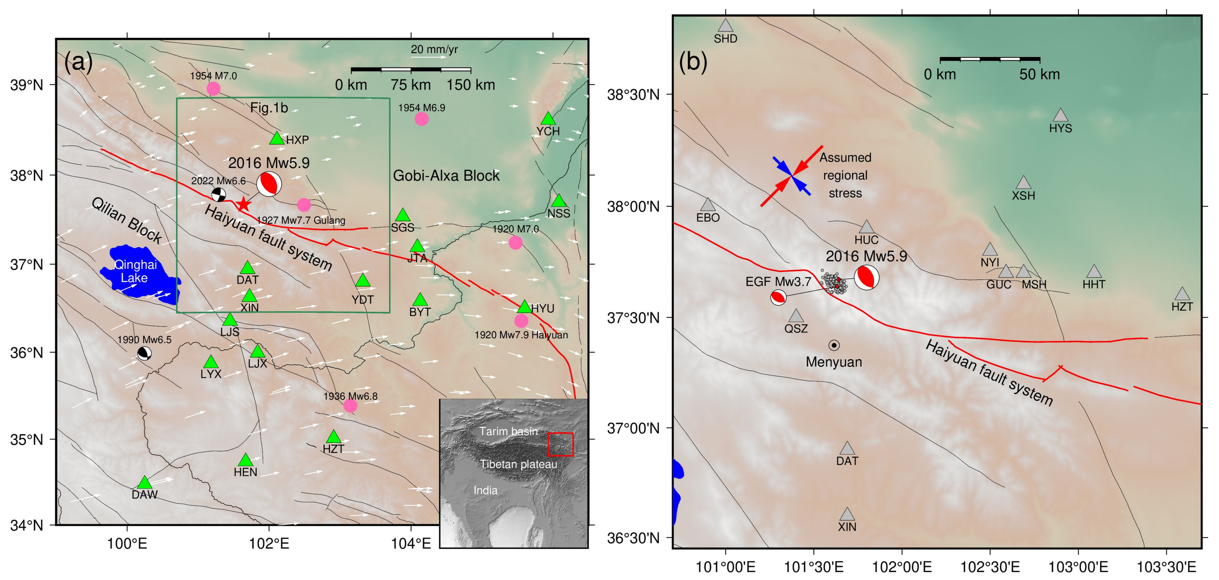

Fig. 1. Tectonic setting of the Menyuan earthquake in the northeastern Tibetan plateau. (a) The broadband stations used in the deconvolution for the apparent source time functions are shown as green triangles. (b) Strong ground motion stations used for waveform comparisons are shown as gray triangles.

2. Point-source focal mechanisms

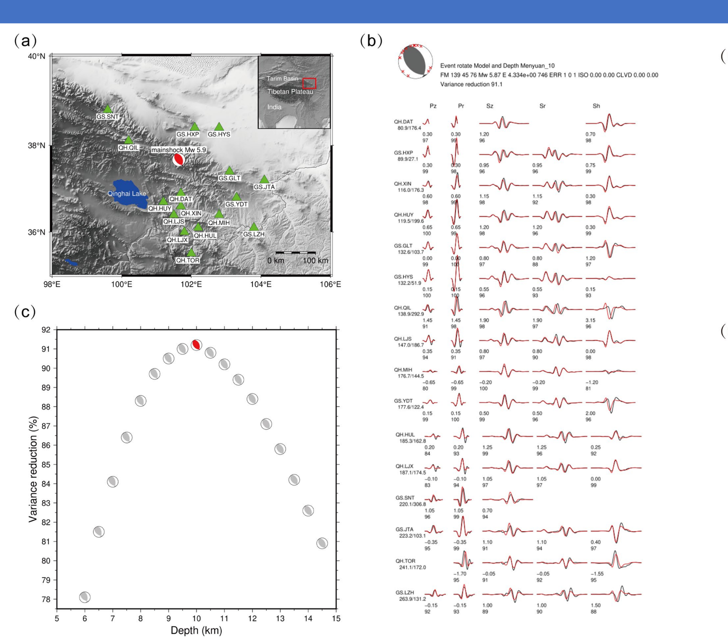

Fig. 2. The point-source focal mechanism inversion for **the Menyuan mainshock**. (a) Broadband seismic stations used for the inversion are shown as green triangles. (b) A comparison between the observed (black) and synthetic (red) waveforms for the solution at the optimal depth of 10 km. P-wave seismograms are bandpass filtered between 0.02 and 0.15 Hz, and S-wave seismograms are bandpass filtered between 0.02 and 0.1 Hz. (c) The variance reduction varies in depth from 6.0 to 14.5 km.

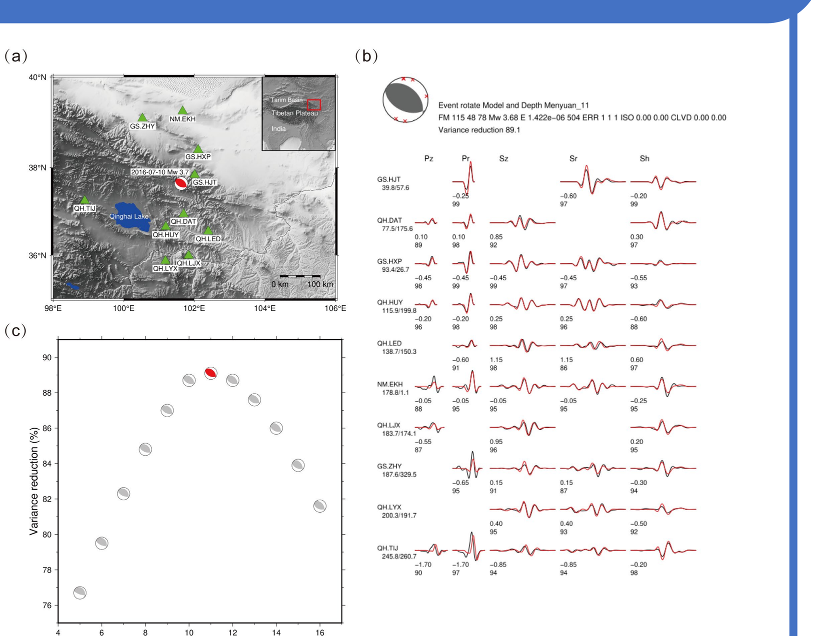

Fig. 3. The point-source focal mechanism inversion for **the EGF event** (2016-07-10, Mw 3.7). (a) Broadband seismic stations used for the inversion are shown as green triangles. (b) A comparison between the observed (black) and synthetic (red) waveforms for the solution at the optimal depth of 11 km. P-wave seismograms are bandpass filtered between 0.03 and 0.15 Hz, and S-wave seismograms are bandpass filtered between 0.03 and 0.1 Hz. (c) The variance reduction varies in depth from 5.0 to 16 km.

1. For the 2016-07-10 event, it has a similar focal mechanism solution (strike/dip/rake = 115º/48º/78º) with the mainshock (strike/dip/rake = 139º/45º/76º).
2. The centroid depth of this event is 11 km, which is close to the 10 km centroid depth for the mainshock.
3. The event is 2.1 orders of magnitude (Mw 3.68) smaller than the mainshock (Mw 5.87).

All of these are favorable conditions for the empirical Green's function method.

Acknowledgments

This work was funded by National Key R&D Program of China (2021YFC3000700), National Natural Science Foundation of China (U1901602, 42174057), and Guangdong Provincial Key Laboratory of Geophysical High-resolution Imaging Technology (2022B1212010002).

3. Apparent Source Time Functions (ASTFs)

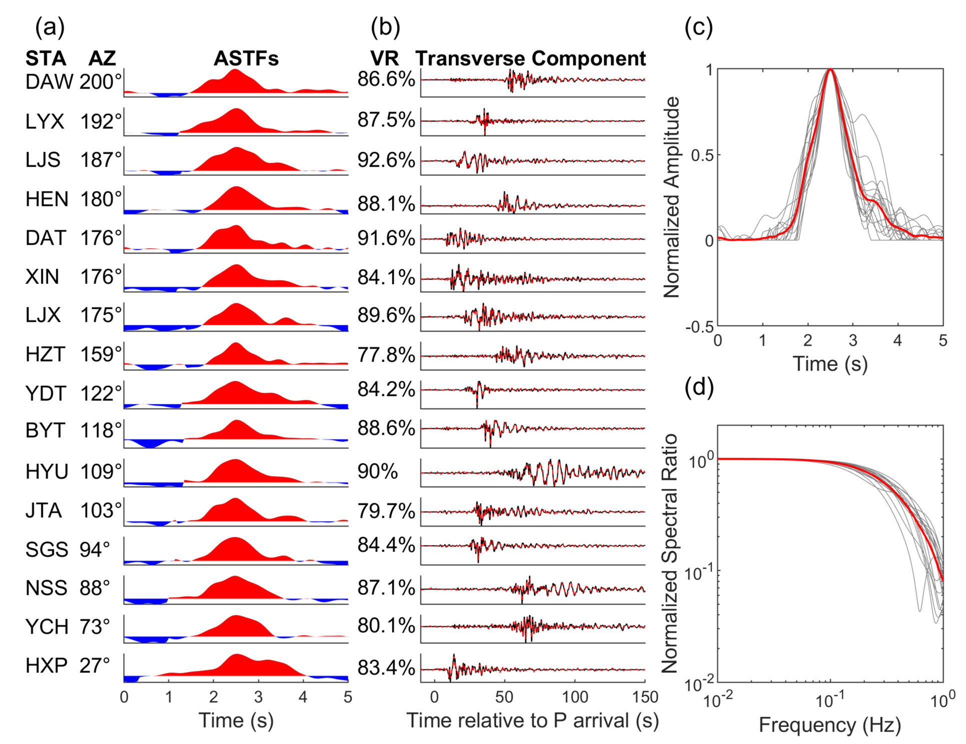

Fig. 4. ASTF deconvolutions of SH waves for the mainshock. (a) ASTFs for the mainshock, and the deconvolutions were done by multitaper spectrum analysis with a 1 Hz lowpass filter. (b) Reconstructions of the mainshock SH waveforms by convolution of the EGF waveform with ASTFs. The black and red curves represent the observed and synthetic SH waves of the mainshock, respectively. (c) Normalized ASTFs (gray lines), and (d) normalized spectra for ASTFs (gray lines) for each station. The red lines indicate the average apparent source time function and the average spectra.

1. One peak of ASTFs is visible at all sites, and the total durations are nearly consistent for different stations, which indicates the rupture directivity is weak.
2. The average apparent source time function (the red line) displays a bell shape, implying that the mainshock ruptures on a single asperity and the rupture process is relatively simple.
3. The spectra of ASTFs are smooth and have no spectral troughs.

4. Dynamic Rupture Simulations

We conduct **two end-member spontaneous rupture models**, namely the runaway rupture and the self-arresting rupture, to further investigate the stopping mechanism of this earthquake, and try to explain the characteristics of ASTFs. The curved grid finite difference method (CG-FDM) [12] is used to simulate the spontaneous rupture process.

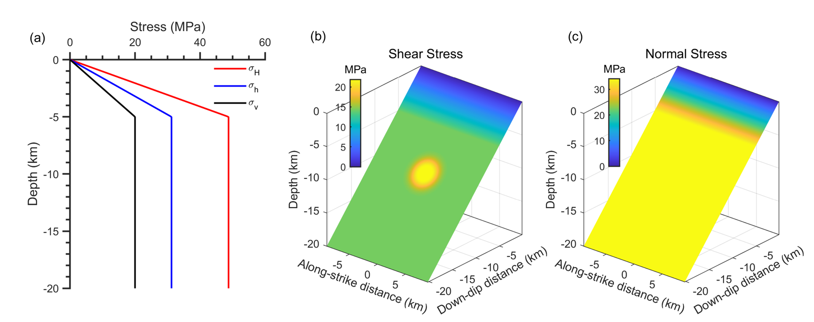

Fig. 5. (a) The distributions of the three principal stresses vary with depth. The distributions of (b) the initial shear stress and (c) the initial normal stress on the fault plane.

Table 1. Parameter values used for the dynamic rupture simulations

Parameter name	Value
Element size	100 m
time step	0.007 s
Nucleation radius	1 km
Static friction	0.64
Dynamic friction for the self-arresting rupture	0.36
Dynamic friction for the runaway rupture	0.26
Slip weakening distance	0.17 m
Maximum horizontal stress	48.76 MPa
Minimum horizontal stress	31.21 MPa
Vertical stress	19.99 MPa
Azimuth of the maximum horizontal stress	N45ºE

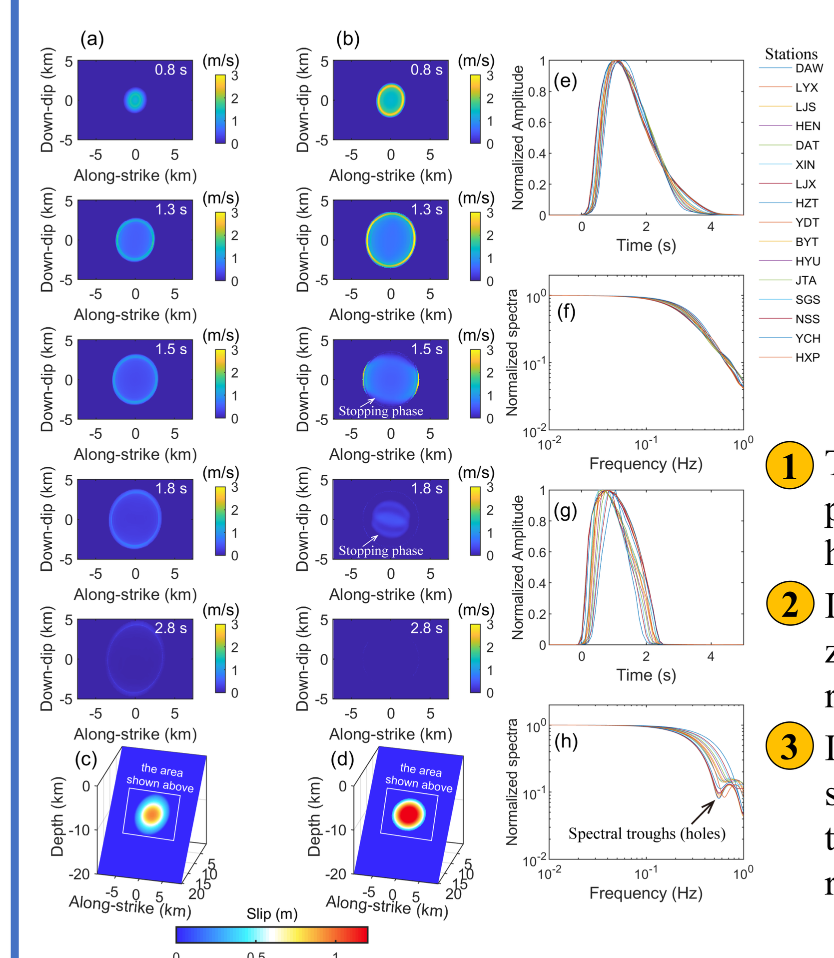

Fig. 6. The rupture process, the final slip, and corresponding ASTFs for different models. For the self-arresting rupture, (a) the rupture propagation at different times, (c) the distribution of the final slip, (e) the normalized ASTFs, and (f) the corresponding normalized Fourier spectra. For the runaway rupture, (b) the rupture propagation at different times, (d) the distribution of the final slip, (g) the normalized ASTFs, and (h) the corresponding normalized Fourier spectra. Differently colored lines represent the different stations shown in Figure 1a (green triangles).

1. The runaway rupture model exhibits a stopping phase, while the self-arresting rupture does not have a stopping phase.
2. In the time domain, the ASTFs gradually drop to zero for the self-arresting rupture. However, for the runaway rupture, the ASTFs drop sharply to zero.
3. In the frequency domain, the ASTFs spectra for the self-arresting rupture are smooth. In contrast, troughs are visible in the ASTFs spectra for the runaway rupture.

5. Surface Deformations and Strong Ground Motions

To check the reasonableness of the dynamic rupture simulations, we compare the predictions of the dynamic sources with geodetic and strong motion observations.

The self-arresting rupture model

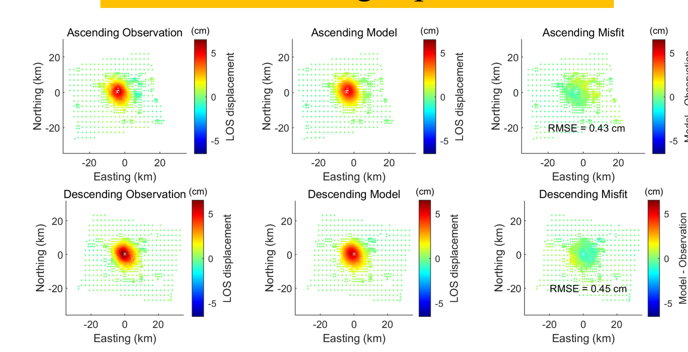

Fig. 7. Comparison of surface deformation observations and predictions for the self-arresting rupture model. The RMSE represents the root mean square error.

The runaway rupture model

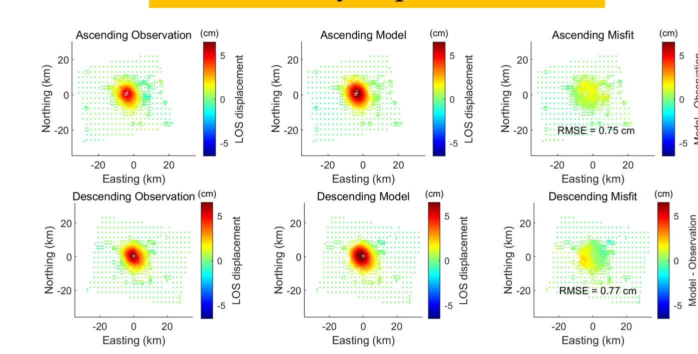

Fig. 8. The same as Fig. 7, but for the runaway rupture model.

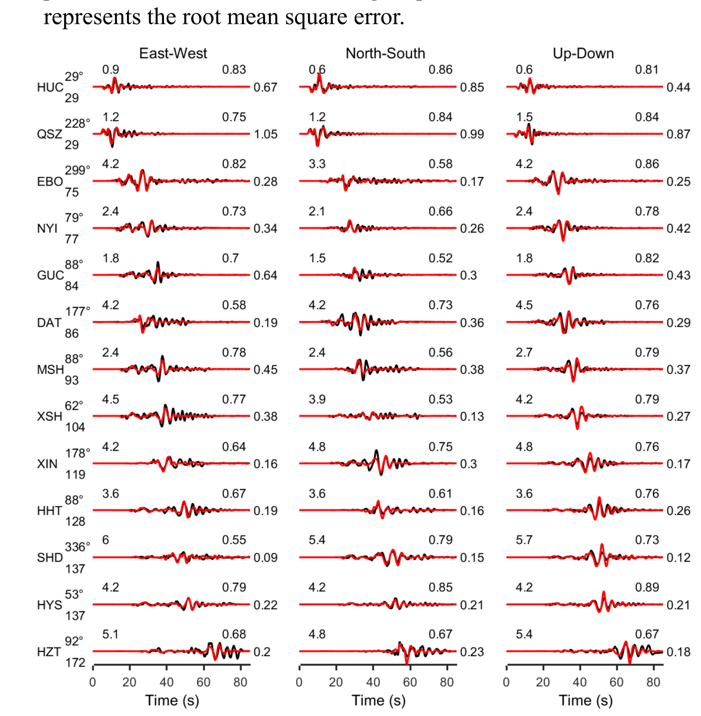

Fig. 9. Comparisons of strong motions between observed (black) and predicted (red) waveforms for the self-arresting rupture model. All the data and synthetics are band-pass filtered between 0.02 and 0.3 Hz. The numbers above the waveforms are the time shifts (left) and the cross-correlation coefficients (right). The maximum absolute values of each component of the observations (cm/s) are listed at the end of each waveform.

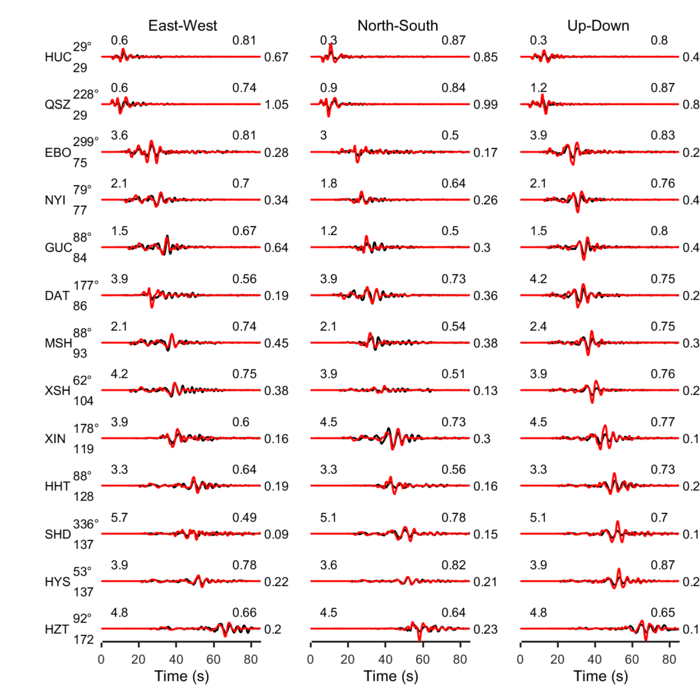

Fig. 10. The same as Fig. 9, but for the runaway rupture model.

1. There is a good agreement between the InSAR observations and the predictions for the self-arresting rupture and a slightly bad fit for the runaway rupture.
2. The synthetics fit well with the observations at most sites for the amplitudes and phases.
3. The wave amplitudes caused by the runaway rupture are larger than the observations, while those caused by the self-arresting rupture are nearly consistent with the observations.

6. Summary

- The ASTFs of the 2016 Mw 5.9 Menyuan earthquake display a single approximate symmetrical peak, and it has a total duration of about 3s (Section 3).
- The spectra of ASTFs have no spectral holes, which can be explained by the self-arresting rupture model (Section 3 and Section 4).
- The dynamic rupture simulations are constrained by the InSAR data and strong ground motion observations (Section 5).
- These results indicate that the 2016 Menyuan earthquake might be a self-arresting event, which highlights the fact that the ruptures of some moderate earthquakes might gradually stop without external barriers.

References

[1] Wesnousky, S. G. (2006). Nature. [2] Elliott et al. (2015). Geophysical Research Letters. [3] Hu et al. (2016). Journal of Geophysical Research: Solid Earth. [4] Xu et al. (2023). Nature Geoscience. [5] Xu et al. (2015). Geophysical Journal International. [6] Galis et al. (2017). Science advances. [7] Wen et al. (2018). Geophysical Research Letters. [8] Wei et al. (2021). Nature communications. [9] Xiong et al. (2019). Pure and Applied Geophysics. [10] Zhang et al. (2020). Seismological Research Letters. [11] Luo & Wang. (2022). Geophysical Research Letters. [12] Zhang et al. (2014). Geophysical Journal International.

Contact me

Duyuan Xu - PhD candidate

Email: xudy_cas@163.com

X2.43 EGU23-6521

This presentation participates in OSPP

Outstanding Student & PhD candidate Presentation contest

Sharing is encouraged